

**EMC2**

<GCUSPIL.T3;vers 3; 07/31/92>

2

**AD-A257 942**



**Electron Recirculation In Electrostatic  
Multicusp Systems: II - System Performance  
Scaling Of One-Dimensional "Rollover" Wells†**

Robert W. Bussard and Katherine E. King

EMC2-0791-04

**DTIC**  
**ELECTE**  
**NOV 23 1992**  
**S B D**

APPROVED FOR PUBLIC RELEASE  
DISTRIBUTION UNLIMITED

CLEARED

OCT 09 1992 4

DIRECTORATE FOR FREEDOM OF INFORMATION  
AND SECURITY REVIEW (OASB-PA)  
DEPARTMENT OF DEFENSE

† This work performed under Contract No. MDA-972-90-C-0006 for  
the Defense Advanced Research Projects Agency, Defense Sciences Office.

42313b  
**92-29995**



REVIEW OF THIS MATERIAL DOES NOT IMPLY  
DEPARTMENT OF DEFENSE INDORSEMENT OF  
FACTUAL ACCURACY OR OPINION.

**EMC2** ENERGY/MATTER CONVERSION CORPORATION  
9100 A Center Street, Manassas, VA 22110, (703) 330-7990

92

92-5-4385

## I. INTRODUCTION AND BACKGROUND

In an earlier paper<sup>1</sup> (hereinafter referred to as "[I]"), a comprehensive study was made of the recirculation and losses of electrons in their flow through simple inverse power-law potential wells bounded by similarly inverse power-law dependent magnetic fields. This study examined electron flow and loss behavior in the simplest approximation invoked to describe Polywell<sup>tm</sup> confinement systems. The importance of this study, and of the present paper, is that the power balance in Polywell<sup>tm</sup> systems is determined entirely by the rate of electron losses; if these are large, then the system can not yield net power.

Thus it is of interest to determine those conditions that result in small losses, and to design experiments and systems to attempt to achieve and operate at these most favorable conditions, in order to test and prove the efficacy of the system for the generation of net power from fusion reactions. The outline and summary of this problem presented in [I] is generally repeated here, with some modifications to clarify particular physics issues of most concern, in order to avoid having to refer to the earlier document for this general description.

As noted in [I], a large body of work has been undertaken over the past 35 or so years in the study of general cusp confinement of plasmas<sup>2, 3, 4, 5</sup>. Nearly all of this has examined single particle electron (or ion) motion or the motion of particles in neutral plasmas within cusped magnetic systems, generally without internal electric potential fields. Furthermore, almost all of this work on plasmas has been limited to plasmas in local thermodynamic equilibrium (LTE); none applied to non-neutral systems. Nearly all were without internal E fields; all particles studied were at constant (fixed) total kinetic energy throughout the system. And, almost all of the prior work focussed on spindle-shaped biconic cusps<sup>6</sup> – which are uniquely unable to satisfy the configuration

criteria necessary for effective electron confinement in Polywell<sup>tm</sup>-type multicusp systems.

These special polyhedral configurations<sup>7, 8</sup> allow formation of stable deep electrostatic potential wells in electron/ion mixtures by radial injection of energetic electrons into plasmas with net negative charge. Their spatial characteristics combined with the distribution of the internal E field arising from electron injection, and the induced predominantly-radial ion motion, can result in long confinement times (due to many recirculation passes through the well before escape) for the electrons<sup>9</sup>. This is the *sine qua non* for minimum electron energy losses, under the conditions of large ion energy and core density achieved by the trapping of ion motion by the electron-driven internal potential.

Although not directly relevant, due to lack of internal potential wells and associated E fields, the work of Taylor<sup>10</sup>, Grossman<sup>11</sup> and Kaye<sup>12</sup> is of particular interest to illustrate some features of the loss situation. Taylor's study suggested that particle losses from spindle cusp systems would be such that the loss rate through the polar cusps would be equal to that through the equatorial ring cusp around the configuration. His result (shown earlier by Grad<sup>13</sup>, and by Berkowitz<sup>6</sup>) was predicated on the assumption that only two constants of the motion exist; the kinetic energy and the angular momentum of the particles. Unfortunately, since this is not the case in the Polywell<sup>tm</sup> or any other symmetrical cusp system, the results derived are of no relevance to the current problem.

A better picture and clear description and analysis of the realistic situation for fixed energy particles in spindle cusps was given by Kaye,<sup>14</sup> who showed that a third constant of the motion, the magnetic moment, acted to reduce the loss rates drastically from those derived under the less restrictive (and incorrect) assumptions of the other analyses. This illustrates the fact that much of the historical work on "cusp confinement" is not of relevance to the problem in Polywell<sup>tm</sup> systems. Conclusions, perceptions, and

or
<input checked="" type="checkbox"/>
<input type="checkbox"/>
<input type="checkbox"/>
n
n/
by Codes
and/or
Special

DTIC QUALITY INSPECTED 4

Dist  
A-1

"understanding" drawn from this body of work are often not applicable to the configurations and particle motions of interest here. In short, "conventional wisdom" in the "fusion plasma community" concerning cusp confinement behavior is frequently of no value as a guide here.

In this note the problem of electron motion, confinement and losses is analyzed in the non-LTE, electron-rich plasma system with anisotropic radial energy in both species, in multicusp Polywell<sup>tm</sup> geometry. The bulk problem is treated as one-dimensional, with arbitrary spatial indices of radial B and E field variation. Here, unlike [I], the B field is taken to have a "rollover" shape, consistent with the results of computer calculations of actual field distributions in polyhedral systems, that follows a simple power-law within the system but departs from it as the system boundary is approached from within. Figure (1), taken from work of Lovberg, Weggel, et al reported by Krall<sup>15</sup> illustrates this in showing the field variation on a major cross-section through a truncated cube system.

An important feature of the Polywell<sup>tm</sup> system is the possibility of inducing B field distortion by bulk diamagnetic collective effects arising from diamagnetic currents induced in the motion of electrons by their interaction with the basic field geometry. These diamagnetic currents will act to exclude the B field from the interior of the system; an effect which will lead to a B field shell, compressed to a  $\beta = 1$  condition, surrounding and confining the central electron cloud in the system. These effects are crudely modelled as they influence this 1-D spatial variation of B field, but electron entry into single cusp volumes includes elements of the geometric effects of the real 3-D configuration. Electron motions in mirror reflection regions are analyzed on the usual basis of conservation of magnetic moment of the electron at entry into the confining cusp. However, turning points of this motion are modified to account for the effects of diamagnetic currents on this process. Further details are given in the following sections.

## II. CUSP MOTION: PROCESS DESCRIPTION AND TECHNICAL APPROACH

There are two distinctly different ways to operate the system. In discussing these it is helpful to define several terms for critical radii within the system. In either case, the electrons are modelled as originating at the system center, at  $r = 0$ , moving through a non-adiabatic region to that radius ( $r_b$ ) at which the electron " $\beta = 1$ ", thence to that radius ( $r_{ad}$ ) at which electrons are captured adiabatically in the cusp fields, and finally to the outer radius,  $r = R$ , of the system.

The first operating scheme is to establish the system with maximum B field, and turn on a small electron current at maximum (desired) electron energy, followed by injection of ions controlled so as to yield the desired central virtual anode height in the system. It has been shown by Bussard and King<sup>16</sup> that this control must be relatively precise (e.g. within a factor of 2-4x) in order to avoid "blowout" of the well by excessive ion density. Given a controllable ion source, and similarly controllable electron injection, the system can be driven to higher core density by injection of ever-increasing electron current with corresponding ion input.

This mode of operation ensures that the system will start as a mirror confinement system for, at low electron density,  $\langle r_b \rangle = (r_b/R)$  is very small compared to  $\langle r_{ad} \rangle = (r_{ad}/R)$  and the only physics initially able to retain the electrons is that of reflection in the cusp fields; no diamagnetic  $\beta = 1$  fields have yet been established. Once started in this mirror reflection (MR) mode, continued increase in electron injection current drives the  $\beta = 1$  radius,  $\langle r_b \rangle$ , to larger values so that some internal reflection within the diamagnetic sphere adds to the confinement due to continuing MR effects. It is important to note that the electron recirculation due to the MR contribution is severely

limited by the considerable depth of the negative potential well created by the (desired) excess electron charge in the system.

In contrast with electron motion under conservation of magnetic moment in field-free cusp systems, the confining effect of the magnetic moment conservation process is greatly reduced here by the presence of the internal E field. This acts to accelerate the electrons outwards in the system, and adds radial energy to their motion almost as fast as the cusp-trapped transverse energy increases and takes it from radial motion. In fact, if the well depth were to become exactly equal to the electron injection energy (a physical impossibility so long as ions are present), the cusp fields would not confine the electrons at all. The MR mode works, but only poorly if the system has a deep potential well.

The general model of electron motion in the system for this mode of startup and operation was discussed and illustrated further in [I], which showed the linear approximation used for variation of the adiabaticity radius,  $\langle r_{ad} \rangle$ , in modelling the transition from the MR mode to the diamagnetic  $\beta = 1$  mode. Examining this mode in some more detail, once the electrons have reached a radial distance ( $r_x$ ) at which their local gyro-magnetic radius is sufficiently small that the total area of all of their gyro radius circles from each of the cusps is equal to the area of the spherical surface at that radius, they will enter one or another cusp in their outward motion. If  $r_b$  is less than this "transition radius"  $r_x$  the electrons move non-adiabatically without confinement, and enter the spatial domain of each cusp at  $r_x$ . No diamagnetic effects are yet functional at this point, as the gyro radius of electrons within  $r_b < r_x$  is greater than the gyro radius at  $r_x$ , and coherent currents counter to the external B fields can not be generated and sustained.

Once  $r_b$  becomes greater than  $r_x$  the electrons inside  $r_b$  will "see" a lossy sphere with surface loss area (due to gyro radius area "holes") that is smaller than the sphere area

at  $r_b$ , and they will be confined by internal reflection within this diamagnetic  $\beta = 1$  sphere. The average number of transits an electron will make within this sphere at  $r_b$  is just the ratio of the sphere area to the total loss area. As  $r_b$  grows larger (with increasing electron current input, and increasing central density – with requisite additional ions to maintain charge balance) this confinement grows larger, because the fractional hole loss area becomes smaller due to increasing B field strength at larger radial positions. This can be thought of as the confinement of a particle inside a perfectly-reflecting spherical shell perforated by holes – like the "wiffle ball" toy; and it is called "wiffle-ball" (WB) confinement. The average number of transits within  $r_b$  is defined here as  $G_{jwb}$ .

At some radius ( $r_{ad}$ ) set by the mirror adiabaticity requirement that the local B field change only little over a local gyro radius, the electron is trapped in "mirror-reflection" (MR) oscillation within the cusp. Electron trapping in this (MR) mode is by the usual form of mirror reflection coefficient for motion in a single cusp mirror system<sup>1\*</sup>. This can be used to find a measure of the average number of transits  $G_{jmr}$  that an electron will make between  $r_{ad} < r < R$  within this cusp mirror geometry.

---

<sup>1\*</sup> The form for mirror reflection coefficient involves a term which is the square of the sine of the minimum trapping angle (relative to the B field) of electron motion in the B field at  $r_{ad}$ , the trapping radius, for their escape at radius  $r = R$ . In the case of a system with electrons at constant energy and a B field varying as  $\langle r \rangle^m$  this term varies as  $\langle r_{ad} \rangle^m$ . In the present case, the simultaneous radial variation of the E field reduces the reflection coefficient by virtue of the acceleration of electrons out of the system by the potential well gradient. If this E field is equal in magnitude to, and varies with the same functional form as the B field, no mirror trapping will be possible in the system. If the potential well is less deep than the electron injection energy, trapping is still possible, but with the reflection coefficient term reduced by a factor of about  $(1 - \alpha_q)$ , where  $\alpha_q = e\Phi_o/E_o$  is the ratio of well depth to injection energy.

As  $r_b$  grows beyond  $r_x$  it begins to distort the externally-imposed polyhedral B field distribution to yield a configuration in which the field is compressed outwards by continuing expansion of the " $\beta = 1$ " surface ( $r_b$ ). This results in the displacement of the adiabaticity radius ( $r_{ad}$ ) to larger radii at a rate such that, with full diamagnetic currents, it will always fall outside the " $\beta = 1$ " radius. Thus  $r_{ad}$  recedes outwards as  $r_b$  exceeds  $r_x$ .

Eventually  $r_b$  and  $r_{ad}$  reach a critical radius  $r_k$  at which further radial growth of  $r_b$  becomes unstable with respect to  $r$ . This is because the magnetic pressure balance criterion is satisfied for all radii beyond  $r_k$ , once it is reached at  $r_k$ . This radial position is that at which the electron (and ion) density begins to increase rapidly with  $r > r_k$ . Up to  $r < r_k$  both ion and electron density fall approximately as  $1/r^2$  from the core region at radius  $r_c$  with density  $n_c$ . Beyond  $r_k$  both ion and electron density increase rapidly, and the electron energy increases while the ion energy decreases as  $r \rightarrow R$ . Beyond  $r_k$  the electron density diverges markedly from the ion density in order to satisfy Poisson's equation and produce the desired negative potential well.

Once  $r_b = r_k$  on this model, the behavior of the system "jumps" from  $r_k$  to  $R$ , where all further increase in system density buildup (by increasing electron and ion injection currents) is stopped at the levels relating drive current ( $I_e$ ) and core density ( $n_c$ ) attained at the  $r_b = R$  condition. This is (obviously) because  $r_b$  can not physically become greater than  $R$ , even though mathematically this is possible, because the B field falls past  $r > R$  and the electron loss area thus increases with increasing  $r$ .

In short, the B field can not confine electrons at a density above that at which the surface electron energy density exceeds the energy density of the magnetic field system. Operation at this final condition is pure WB mode, and is at the point where  $\langle r_b \rangle = 1$ ; all

mirror effects have vanished and the electron confinement is due entirely to recirculation within the diamagnetic sphere perforated by loss holes on the cusp axes whose radii are proportional to the on-axis strength of the cusp B fields.

This final  $\langle r_b \rangle = 1$  WB mode operating condition can be reached by an alternate route. The other extreme of startup and operation is to avoid the MR mode entirely, and drive the system from the beginning as a high beta diamagnetic device. This can be done, in principle, by starting with any desired electron injection energy but with a greatly reduced B field, so that the  $\beta = 1$  surface initially is very far out in the system,  $\langle r_b \rangle \approx 1$ . At this condition there will be no mirror reflection, because there is no mirror field region; all of the field is diamagnetically compressed to the outer boundary region, and all electron losses are governed by the WB gyro hole loss mechanisms (see e.g. Kaye).

However, with small B fields and large electron energy (as required for the production of wells deep enough to yield ions with high fusion cross-sections) the electron recirculation factor ( $G_{j_0}$ ) will be very much too small to achieve low electron losses and good power balance. In order to reach high  $G_{j_0}$  values the confining B field, that sets the size of the electron gyro loss holes in the WB sphere, must be increased to a much larger value.

If this is done rapidly, with no increase in electron current, the  $\beta = 1$  sphere will be compressed to a radius smaller than  $r_b \approx R$ , and the WB confinement will be reduced by the increase in gyro hole loss area due to the decreased gross B field at smaller radius, as well as by the smaller size of the confining sphere. If this decrease is sufficiently large, the system will reach an unstable mode such that the WB sphere will continue to shrink until it stabilizes with the rise of MR mode confinement as  $r_b$  falls below  $r_k$ . Now, the system has "jumped" to operation in the MR mode, as described above.

However, if the B field is increased slowly (relative to electron lifetime in the system), and in small steps, the system will remain stable along the  $\langle r_b \rangle = 1$  line and can be driven to higher and higher recirculation simply by increasing the B field, without increasing the electron drive current. This method avoids the limiting behavior of the MR mode, and allows attainment of the final state of maximum  $G_{j_0}$  on the  $\langle r_b \rangle = 1$  line with much less drive current that is required to make the transition from MR to WB mode in the other startup scenario.

In either case, at this final stable state, when  $r_b = R$  the core and bulk densities of electrons (and also of ions) are at their maximum values for the parameters defining the system (e.g.  $I_e$ ,  $n_c$ ,  $E_o$ ,  $B_o$ ,  $R$ ). Further increase in electron drive current can not increase system density. Since fusion power output is proportional to the square of the core density, and since this is proportional to the surface density – and hence to the square of the B field – it is clear that increasing B field strength has a strong effect on system fusion power generation. On this simple argument, on the  $\langle r_b \rangle = 1$  line, the fusion power will vary as the fourth power of the B field, just as for conventional magnetic confinement machines.

In the MR startup case, when electron injection is started, the only confining mechanism is mirror–reflection (MR) from the radius  $r_{ad}$  to  $R$ , over a number of transits  $G_{jmr}$ . As electron injection current is increased the WB mode develops when  $r_b > r_x$ , and the confinement parameter  $G_{jwb}$  grows progressively larger than unity. Particles between  $r_{ad}$  and  $r_b$  simply transit through this space. Since all particles that emerge from  $r_b$  (escaping the WB region) enter the MR region at  $r < r_{ad}$ , the total number of passes that an electron will make before loss is the product of those in each region.

In order to describe behavior of the "average" electron in the system,  $G_j$  in each region must be weighted by the number of particles in that region. For the  $1/r^2$  density

variation previously cited, this weighting is simply proportional to the region radial extent, running over  $0 < r < r_b$  for the WB region and  $r_b < r < R$  for the MR region. This simple weighting neglects the density increase in the region  $r > r_k$ , and thus underestimates the MR contribution when  $r_b < r_k$ , and the WB contribution when  $r_b > r_k$ . In the WB startup case, only the wiffle-ball parameter  $G_{jwb}$  will be active, and this will characterize electron motion across the entire extent of the machine.

The behavior of electron losses is determined entirely by the lifetime of electrons in the system. This lifetime can be related to the average transit time of the "average" electron, weighted over the transit times of the electrons across their radial and transverse energy distribution, and the average number of transits,  $G_{jo}$ , which is the electron recirculation factor. This can be found by analysis of the time spent in the MR mode and adding this to that spent in the WB mode and dividing this total system lifetime by the average electron transit time in one pass through the system. This average transit time must be estimated as correctly as possible to obtain correct models of cusp losses. The final parameter of interest is the recirculation,  $G_{jo}$ , as this is described in terms of design specifications of the system.

As discussed in [I], this analysis is difficult because of the somewhat complicated electron distribution in both radial and transverse energy, and by the non-monotonic nature of the potential well, which involves both a central virtual anode and a "rollover" at the system boundary. This latter feature was not incorporated in the model used in [I]; it is included in the analysis here. Details of the methods used to determine transit time are discussed in [I], and in an earlier EMC2 technical report. These same methods were employed here, with the addition of the complexities of the rollover field and a parameter describing the well depth in terms of the electron injection energy.

Figure (2) summarizes the mathematical formulae obtained from this analysis, giving transit times in different regions of the potential well in terms of parameters describing the well shape and critical radial points across the device. Note the explicit dependence of transit time on the well depth parameter,  $\alpha_q = e\phi_o/E_o$ , as well as on the modified virtual anode height parameter,  $\eta' = 1 - \alpha_q(1-\eta_o)$ . Transit times are determined by integration over each of these forms, in the regions in which they are applicable.

### III. ANALYTIC MODELS OF ELECTRON MOTION

In [I] the electron motion was based on a simple monotonic potential well with magnetic field and electron kinetic energy variation according to

$$B(r) = B_o \langle r \rangle^m \quad \text{and} \quad E(r) = E_o \langle r \rangle^m \quad (1)$$

where  $\langle r \rangle = (r/R)$ . However, studies<sup>17, 18, 19</sup> have shown that the field variation asymptotically approaches the simple power law form only as the radius becomes smaller (approaching the origin) within the system. At radii beyond about  $\langle r \rangle = 0.5$ , the field modulus exhibits a "bumpiness", and its variation in any plane section through the center of the system and one of the edge midpoints always shows a "rollover" as the edge of the system is approached. Figure (1) shows an example of this sort of variation with radial position.

The effect of this realistic departure from the power law assumed in [I] is beneficial to electron confinement because it gives larger B fields at deeper radii than does the simple power law (for the same face cusp central field strength). The simple model is thus likely to yield results that are conservative (or pessimistic), because of its underestimate of the strength and effects of the real magnetic fields in the system. This can be rectified by

employing an improved description of the B field, which better mocks up the actual variation within the polyhedron. Limiting this, as before, to radial-only dependence (1-D can be analyzed in closed form; 2-D can not) it is found that the edge effects can be accounted for in an approximate way by use of

$$B(r) = B_0 \langle r \rangle^m f_0(r) = B_0 \langle r \rangle^m \left[ \frac{2}{(1 + \langle r \rangle^{m+2})} \right] \quad (2)$$

It is obvious from this that the field strength deep within the system will be twice that previously used, for the same value of cusp central-axis maximum field strength,  $B_0$ . As a result, the electron gyro radii at these inner radial positions will be roughly one-half of those previously estimated, with concomitant improvement in electron confinement.

This simple formula has the advantage that it will still yield analytic solutions for most (but not all) of the parameters which characterize the system and are used in the solution methods employed in the model of [I] (e.g. the specific dimensionless radii  $\langle r_{ad} \rangle$ ,  $\langle r_b \rangle$ ,  $\langle r_x \rangle$ , and the separate mode recirculation ratio terms  $G_{jmr}$  and  $G_{jwb}$ ). Unfortunately, the transit time integrals can not be obtained in useful closed forms with this more realistic potential variation. However, since the transit time segments used in the calculation of the electron recirculation are divided by the total transit time in the expression for the overall system  $G_{jo}$  ratio, the effect of integral departures from exact behavior are minimal for this factor, thus these times can be taken from the forms described above (and shown in Figure 2) without serious error.

Consider the motion of electrons in this rollover well, under adiabatic conditions where the magnetic moment,  $\mu_0$ , remains constant. Here the total energy of the electron is

$$E_{tot} = E_p + E_k = E_p + E_{perp} + E_{para} \quad (3)$$

where  $E_p$  is the potential energy in the E field, and  $E_k$  is the kinetic energy of motion, divided into its two component,  $E_{perp}$  and  $E_{para}$ . Also, the magnetic moment of any given electron is related to its  $E_{perp}$  relative to the field and to the B field and well depth parameter by

$$\mu_o B_o \langle r \rangle^m = E_{perp} = E_o \sin^2(\Theta_{ad}) \langle r/r_{ad} \rangle^m [1 - \alpha_q (1 - \langle r_{ad} \rangle^m)] \quad (4)$$

where  $\Theta_{ad}$  is the angle of entry of the electron into the adiabatic cusp at  $\langle r_{ad} \rangle$  and  $\alpha_q = e\phi_o/E_o$ , as before. Using this in eq. (3) and taking the kinetic energy to be  $E_k = e\phi_o(1 - \langle r \rangle^m)$  allows determination of  $E_{para}$ . Setting this equal to zero, to determine the mirror reflection condition for the given electron yields a restriction on the angle of entry of electrons into the adiabatic field as

$$\sin^2(\Theta_{ad}) = \frac{[1 - \alpha_q (1 - \langle r \rangle^m)] \langle r_{ad} \rangle^m}{[1 - \alpha_q (1 - \langle r_{ad} \rangle^m)] \langle r \rangle^m} \quad (5)$$

Now, the electrons will arrive at  $\langle r \rangle = 1$  at the system edge. Thus, the entry angle which yields such a reflection can be determined from eq. (5) by setting  $\langle r \rangle = 1$  and solving for  $\sin^2(\Theta_{ad})$  to give the minimum angle possible for electron trapping. This is found to be  $\Theta_{min} = \sin^{-1} [\langle r_{ad} \rangle^m / (1 - \alpha_q (1 - \langle r_{ad} \rangle^m))]^{0.5}$ . Eq. (5) can then be integrated over the range of angles from which electrons enter the cusp region at  $\langle r_{ad} \rangle$ , and normalized to the total angle, to find the effective reflection coefficient. Carrying out this integration (from  $\Theta_{min}$  to  $(4/N)^{0.5}$ ) gives the electron reflection coefficient [R] in terms of the number of cusps N, the well parameter  $\alpha_q$ , and the adiabaticity radius  $\langle r_{ad} \rangle$ . The recirculation due to mirror reflection is just  $G_{jmr} = 1/(1-[R])$ , which is

$$G_{jmr} = \frac{4[1 - \alpha_q (1 - \langle r_{ad} \rangle^m)]}{N \langle r_{ad} \rangle^m} \quad (6)$$

This is just the "old" formula for  $G_{jmr}$  used in [I], multiplied by the term due to well depth. Here  $N$  is the (effective) number of point cusps in the system (in a system with all cusps identical,  $N$  is twice the number of full bi-polar magnetic axes).

Similarly, the radius of transition ( $r_x$ ) from uncorrelated to cusp-centered non-adiabatic motion is found by solution of the geometric definition of  $\langle r_x \rangle$  given by  $4\pi(r_x)^2 = N\pi(r_L(r_x))^2$ , where  $r_L$  is the "gyro loss radius", defined as  $r_L = k_L r_g$ . Here  $k_L$  is a measure of the departure of gyro "hole" area losses from the strict single-gyro-radius (minimum) limit. The local gyro radius is

$$(r_g(r))^2 = \left[ \frac{2E_o \langle r \rangle^m}{r_e (B_o)^2 \langle r \rangle^{2m}} \right] \left[ \frac{\sin^2(\Theta_{ad}) (1 - \alpha_q (1 - \langle r \rangle^m))}{(f_o \langle r \rangle)^2} \right] \quad (7)$$

where  $\sin^2(\Theta_{ad})$  must be taken as the mean square of the sine of the entry angles of all electrons into the cusp system, defined as  $S^2$ . As usual, this can be written more compactly in terms of the parameter  $W = E_o / (B_o R)^2$  characterizing the system design, and  $r_e = e^2 / mc^2 = 2.818E-13$  cm is the classical radius of the electron. Note that  $(2W/r_e)$  is the square of the ratio of electron gyro radius at the system boundary to the boundary radius, and is a measure of the "goodness" of confinement; small  $W$  gives longer lifetimes than large  $W$ . With these the transition radius in the unperturbed field is

$$\langle r_x \rangle^{2m+2} = \left[ \frac{NW(k_L)^2}{2r_e} \right] [S^2] \left[ \frac{1 - \alpha_q (1 - \langle r_x \rangle^m)}{(f_o \langle r_x \rangle)^2} \right] \quad (8)$$

Note that this is an implicit equation for  $\langle r_x \rangle$ , which can not be solved analytically. Similarly, the "adiabaticity radius" in the unperturbed field ( $r_{ado}$ ) is defined, for an adiabaticity index<sup>20</sup> ( $\Gamma_a$ ), as

$$[\Gamma_g(r_{ado})] \left[ \frac{d \ln(B(r))}{dr} \right] \Big|_{r_{ado}} = [\Gamma_g(r_{ado})] \left[ \frac{m}{r_{ado}} \right] = \Gamma_a < 1 \quad (9)$$

This, too, yields an implicit equation for  $\langle r_{ado} \rangle$ , in terms of the W parameter and the adiabaticity index, the well depth factor, and the rollover field function  $f_0$  and its first derivative. This equation is given in Figure (3) which contains a summary of all of the equations describing electron motion in this more realistic (than [I]) field and well geometry.

Comparison of the criterion eq. (9) with computer simulation data<sup>21, 22, 23</sup> for electrons of fixed energy shows that  $\Gamma_a \approx (2/3)$  is a reasonable fit to the data for motion in the magnetic field configuration of a truncated cube.

As the electron density builds up within  $r < r_b < r_x$  collective diamagnetic effects initially will be negligible, because the gyro radius at small  $r$  within this region is greater than the dimension  $r$ , itself. Increasing electron density will push  $r_b$  to larger radius and, when  $r_b$  approaches  $r_x$ , the diamagnetic currents due to internal electron gyro motion will begin to affect (reduce) the local B field amplitude. As  $r_b$  exceeds  $r_x$  and approaches  $r_{ad}$ , gyro currents become relatively stronger and more concentrated around the cusp axis, and this relative reduction in B field will increase.

This results in an outward compression of the B field external to the  $\beta = 1$  surface, which will affect the true position of the adiabaticity radius in such a way that the true adiabatic motion condition can no longer be satisfied at its original position  $\langle r_{ado} \rangle$  in the undisturbed field. The adiabaticity radius will move further out into a region of larger B field. The net result is a progressive "pushing" of the effective  $r_{ad}$  to larger radii, by  $r_b$  moving out with higher interior electron density. This pushing displacement can continue

only to the critical density turnaround radius  $r_k$ , at which point  $r_b = r_{ad} = r_k$  and  $r_b$  jumps to  $R$ , as discussed previously. In a general analysis of particle density distributions, Krall<sup>24</sup> showed that the position of  $\langle r_k \rangle$  depends on the the potential well shape. For typical well shapes of interest,  $\langle r_k \rangle \approx 0.83$ . However, note that the distortion of B field introduced by diamagnetic effects will result in a comparable distortion of the potential shape, thus the value of  $\langle r_k \rangle$  will increase towards unity (1) as  $\langle r_b \rangle$  becomes larger, out to  $\langle r_b \rangle = 1$ .<sup>2\*</sup>

This collective effect was modelled (in [I]) crudely by a linear algorithm that scaled the motion of  $r_{ad}$  from  $r_{ado}$  to  $r_k$  in proportion to the motion of  $r_b$  from  $r_x$  to  $r_k$ . This model considerably overestimates the true diamagnetic shift effect. In order to test the importance of the model, calculations were made of systems with this overestimated form and with no diamagnetic shift effect at all. The results are shown in Figures (4a,b) that show the variation of  $G_{j_0}$  with  $Z$  and  $W$  for these two extreme cases. Note that the only difference is in the  $Z$  position at which the mirror component of  $G_j$  begins to decrease, and that this difference is only about a factor of 3x in  $Z$  (the maximum diamagnetic shift gave lower  $Z$  values). As indicated by theory, no effect was found in the WB region.

The " $\beta = 1$ " radius is the radial position at which magnetic pressure exactly balances electron kinetic pressure,  $(n(r_b))(E(r_b)) = (B(r_b))^2/8\pi$ . The variation of particle density with radius from the core density  $n_c$  at  $r_c$  is given by an inverse-square relationship

---

<sup>2\*</sup> However, note that  $\langle r_k \rangle$  can never reach unity in systems with a finite number of cusps, because gross MHD beta stability limits the radius of  $\langle r_k \rangle$  between cusps to that at which the outwardly compressed B field is tangent to the plane passing through the maximum B amplitude point in each surrounding cusp. For an  $m = 3$  (truncated cube) system this limits  $\langle r_k \rangle$  to a maximum value of about 0.883.

out to about  $r_k$ . Using this, the  $\beta = 1$  radius,  $r_b$ , is found to be given by another implicit equation (as for eq. 8, above), in the parameters  $\alpha_q$ ,  $W$ , and the  $f_o$  function, and the new parameter  $Z = 8\pi n_c(r_c)^2$ . The implicit equation for this is shown in Figure (3). Note that  $(Zr_c/6)$  is the total number of ions (or electrons) in the core.

The filling of the system so that  $r_b$  becomes greater than the transition radius  $r_x$  creates a WB confinement sphere with electron recirculation determined as

$G_{jwb} = 4\pi(r_b)^2/N\pi(r_L)^2S^2$ . Using the equations for  $(r_b)$  and  $(r_L)$  gives this as

$$G_{jwb} = \frac{2r_e Z}{N(k_L)^2 S^2} \quad (10)$$

To determine the overall lifetime and mean number of passes made by an electron in the system it is necessary to find these parameters for each mode of confinement, and weight them by the fractional number of electrons participating in each mode. This introduces a weighting factor dependent on  $\langle r_b \rangle$  in the equations given in Figure (3).

The time an electron spends in the MR mode is just that during its transit time  $t_{mr}$  between  $r_b$  and  $R$ , multiplied by the number of MR mode recirculation  $G_{jmr}$ . Note that  $G_{jmr}$  is determined by motion over the radial interval  $r_{ad} < r < R$  or  $r_b < r < R$ , while the transit time includes the non-reflective region  $r_b < r < r_{ad}$ , if such exists. For  $1/r^2$  variation of density, the number weighting function is just  $(1-\langle r_b \rangle)$ . Note that this underestimates the weighting because the density actually increases at  $r > r_k$ . The time spent in the WB mode  $t_{wb}$  is that while transiting the space  $0 < r < r_b$ , multiplied by the number of WB mode recirculation and the number of MR passes for each such recirculation. Its particle number weighting factor is simply  $\langle r_b \rangle$ ; here correct as the density variation with radius is inverse-square in this region.

As remarked earlier, determination of these transit times requires integration over the electron energy distribution in the potential well, for the several regions of the well that apply to each condition. Carrying this out results in the transit time formulae summarized in Figure (2). With these it is possible to write the recirculation ratios for the two cases when the system has not yet begun to exhibit WB mode operation (i.e. when  $r_b < r_x$ ) and when the system does show this mode (i.e.  $r_b > r_x$ ). These formulae are also given in Figure (3).

Using these formulae it is possible to calculate  $G_{j_0}$  over a range of the system-defining parameters, ( $Z$ ) and ( $W$ ). Note that  $W$  is defined by system external design criteria, while  $Z$  is determined by internal conditions reached in the dense core during system operation. It is instructive to examine  $G_{j_0}$  to see how the MR and WB contributions vary with these parameters.

Each of these can be calculated separately from their terms in the overall formulae for  $G_{j_0}$ . Since all of the relevant parametric terms in these equations are given only in implicit form, it was necessary to construct a simple computer code to calculate  $G_{j_{mr}}$ ,  $G_{j_{wb}}$  and  $G_{j_0}$ . This code, called the GJ code, was used to determine parametric scaling of  $G_j$  with  $Z$  and  $W$  for a wide range of operating and design parameters for the Polywell<sup>tm</sup> systems of interest. Results of these calculations are shown in a series of figures attached herewith (Figures 5-8). All calculations were made for a truncated cube system with an effective cusp number of  $N \approx 8$ , a B field spatial index of  $m = 3$ , a critical density radius of  $\langle r_k \rangle = 0.83$ , loss radius factors of  $k_L = 1, 2, 3$ , and for a potential well with virtual anode fractional height of  $n = 0.272$ .

All the figures show that  $G_{j_{mr}}$  drops with increasing  $Z$  (increasing core density) beyond the point where  $r_b \geq r_x$ . This is a result of the decrease in both MR mode time  $t_{mr}$

and in the weighting term  $(1-\langle r_b \rangle)$ , even before  $\langle r_b \rangle$  reaches  $\langle r_{ado} \rangle$ . As  $\langle r_b \rangle$  moves beyond  $\langle r_{ado} \rangle$  the drop is even faster, as the diamagnetic effects of induced counter-currents in the electron flow become larger and "push"  $\langle r_{ad} \rangle$  to larger radii.

The WB mode does not begin until  $r_b > r_x$  and then rises rapidly with increasing  $Z$ ,  $t_{wb}$  and the weighting term  $\langle r_b \rangle$ . This is quite clearly seen where the  $G_{jwb}$  curves fall rapidly to unity as  $Z$  approaches a value of about  $1E14/cm$  from above. The cutoff  $Z$  value is determined from the equation for  $G_{jwb}$  by setting this equal to unity. Thus, for all values of  $Z < N(k_L)^2 S^2 / 2r_e$  the system will be operating solely in the MR mode. This has the inverse consequence that WB mode physics can be tested only if the experimental system is capable of being driven to a core density above this cutoff limit;

$$n_c(r_c)^2 > N(k_L)^2 / 16\pi r_e.$$

Operation along a line of constant  $W$  above this point leads to a maximum  $G_{jwb}$  value at the boundary where  $r_b = R$ ; beyond this point  $G_{jwb}$  no longer increases with greater input electron current. Also, at this point the electron (and ion) density within the system has reached its maximum value and all further density buildup is stopped, for here the system surface is already operating at an electron/magnetic beta of unity; more electrons can not be contained within this field. All of the early studies<sup>15</sup> of this concept were made along this line of maximum performance, at the condition  $r = r_b$ .

The sum of these two terms gives  $G_{jo}$  for the complete system. Figures (5a-f), (6a-d) and (7a-d) show 2-D plots of this total  $G_{jo}$  for  $m = 3$  power-law wells with a virtual anode, over a range of  $Z$  and  $W$ , and for convergence ratio  $\langle r_o \rangle = 1E-2$  and anode height  $\eta = 0.272$ . Figures (5a-f) show a wide range of the well depth parameter  $\alpha_q$ , from zero (no well) to 0.995. Figure (6a) is a plot of just the  $\langle r_b \rangle = 1$  line for several values of the gyro loss radius parameter  $k_L$ . Figures (6b-d) show the full  $G_j$  vs.  $Z$  plots for each

value of  $k_L$  at  $\alpha_q = 1$ , full well at electron injection energy; no MR mode. As expected, increasing  $k_L$  shifts the  $\langle r_b \rangle = 1$  line to higher  $Z$  by a factor of  $k_L^2$ . The repeller effectiveness,  $\alpha_r$ , was also varied over the range from 0 to 0.999 and is shown in Figures (7a-d). As expected, increased repeller effectiveness affects only the MR component of  $G_{jo}$  by the simple multiplying factor  $1/(1-\alpha_r)$ , thus repellers with 0.9 effectiveness will yield 10x electron densities in MR mode operation as compared to a system with no repellers. The variation of repeller effectiveness is also plotted in 3-D in Figures (8a-c). These graphs show clearly the separate MR and WB modes of operation with the large "valley" in between.

Examination of Figures (5a-f) shows that the well depth affects the MR mode drastically as  $\alpha_q$  becomes larger than about 0.8-0.9, and that the character of the parameter phase space changes for larger values than 0.9. In particular, it is found that the MR mode regime bifurcates from the WB mode regime, and develops a characteristic behavior that is antithetical to WB operation. A "valley" appears between these two regimes of operation that subsequent code calculations have shown is very difficult to cross.

Another series of calculations was made to test the effect of anode height on  $G_{jo}$ . These showed that the variation of  $G_{jo}$  with  $Z$  and  $W$  is virtually independent of  $\eta$  for all  $\eta > 0.01$ . At very small  $\eta \rightarrow 0$  the forms used for the transit time integrals begin to break down and give excessive transit times; for all realistic wells the dependence of  $G_{jo}$  on anode height is negligible for  $0 < \eta \lesssim 0.3$ .

It is useful to distinguish three regions of differing character on these figures. In the left hand region below  $Z \approx 1E13/cm$  the electron behavior is completely dominated by mirror-reflection effects. In this area the device is simply a multicusp mirror machine, operating with the usual MR features. In the right hand region above  $Z \approx 1E16/cm$ ,

electron behavior is completely dominated by collective mode (diamagnetic) wiffle-ball effects, and mirror phenomena in this region have essentially vanished. Here and above (to  $Z > 1E18/cm$ ) lies the fusion reactor regime. This region is new and unfamiliar to the field of cusp plasma research; it forms the basis for the original Polywell<sup>tm</sup> concept and the early studies<sup>25</sup> of its characteristics.

In the middle region where  $8E13 < Z < 8E15/cm$  lies all of the physics of transition from MR to WB operation. This region is of experimental and theoretical interest, because of the new and novel physics features found here. However, this transition is significant for operation of these devices in fusion reactor regimes only if the system is started in the MR mode.

A variety of calculations have been made that show the parametric performance across the range from pure WB mode to pure (initial) MR mode. These are summarized for one set of cases on Figures (8a,b,c) that show three-dimensional pictures of the two-dimensional portrayals of the earlier figures. From these it is evident that the device can operate either as a mirror machine OR as a wiffle ball machine, but that it can NOT operate as both.

Examination of the calculated data shows that the MR mode (the right hand area of the figures) leads to increased  $G_j$  but only at modest  $Z$ , not sufficient for power reactor operation. However, starting the system as a WB machine causes it to ride up the  $\langle r_b \rangle = 1$  "ridge" line at the left hand side of the figures, always with an increasing  $G_j$ . Detailed EKXL code calculations have been made, to test the validity of this GJ code global mapping, that show the drive current required to move up either of these startup paths.

The results show that following the MR mode at small  $W$  leads to early increase in  $G_j$ , until  $Z$  values around those of the  $\beta = 1$  line are reached. Beyond this point, to force the machine through the transition from MR to WB modes, in order to get on the  $\beta = 1$  line, itself, requires ever-increasing electron drive currents. In contrast, if the device is started with a large  $W$  (e.g. by operation at low  $B$  field), it can be made to reach the  $\beta = 1$  line at small  $G_j$  in the WB mode, and then to ride up the  $\langle r_b \rangle = 1$  line by slow reduction of  $W$  (by slow increase of the  $B$  field) to the reactor regime (ca.  $Z \approx 1E19/cm$ ) without significant increase in the current required to reach the  $\beta = 1$  line in the first place.

Note that the electron recirculation ratio  $G_{jo}$  increases more slowly with  $Z$ , in the MR mode, once the  $Z$  value has passed that for  $\beta = 1$  (in the 2-D projections), and that the slope of the  $G_{jo}$  vs.  $Z$  curve, along a line of constant  $W$  first becomes negative, then slowly becomes positive, until it reaches a slope of unity. Below this point the system is grossly stable with respect to increasing drive current input. However, beyond this point the slope exceeds unity, and the system becomes grossly unstable. From this point up to the  $\langle r_b \rangle = 1$  line (at which point the device can not be driven further) the current must be reduced, for operation on the  $\langle r_b \rangle = 1$  line requires LESS current than to reach the slope  $< 1$  regions beyond the  $\langle r_b \rangle = 1$  line below the unstable region. This can all be avoided by operation along the  $\beta = 1$  line, as described above.

Since the value of  $G_{jo}$  for MR operation drops with increasing  $Z$ , from its initial low- $Z$  value, as operation leaves the MR mode - before WB mode confinement has taken any significant effect - it appears as a "gate" through which machine operation must be driven at startup. This is true only if started in the MR mode and is NOT true if started in the WB mode. If the device is drive-current-limited, and if the current is insufficient (for the design values of minimum  $W$  for the machine) to yield  $Z$  values (e.g. core

densities) beyond this gate region, it will not operate above the much smaller Z value to which the limited current can drive it in the MR mode.

It is very important to note the effects and characteristics anticipated for this device. In particular, a limited-current experiment operating strictly in the MR mode that runs into the "gate" effect will demonstrate poorer electron (and ion) confinement with increasing current and core density. This is to be expected in this regime. Results of such experiments can map out the MR portion of the 3-D parameter space that describes complete system operation, but can not illuminate the physics of operation in the WB regime. This regime is along the  $\langle r_p \rangle = 1$  ridge line in the parameter space of the system, as shown in Figures (8a,b,c).

This final form of the  $G_{jo}$  formalism outlined above has been developed as a simple computer program, the GJ code. This (GJ vers. 1.1), has been built into the EKXL code (vers. 4.1), so that this code now incorporates fully correct physics models that properly describe system behavior across all the possible range of parameter space.

Calculations using this version 4.1 of the EKXL code have been made parametrically for a variety of cases at high density ("reactor") conditions, and for a wide range of models for SCIF experimental systems and operations. Results of the SCIF computations are discussed in a separate EMC2 technical note<sup>26</sup>. Results of the reactor case studies are given in a forthcoming EMC2 technical note. In all of these the effective "loss radius" has been taken to be in the range  $2 < k_L < 3$ , as derived from elementary considerations<sup>27</sup> of diamagnetic behavior in the system. Knowledge derived from this work has been used to analyze possibilities for startup of SCIF with neutral background gas; this is reported in another technical note.<sup>28</sup>

## LIST OF FIGURES

**Figure 1.**

Variation of magnetic field in pure linear truncated cube systems, showing "rollover" at edge and field strength 2x higher in interior regions than used in simple power-law model normalised to square face edge strength.

**Figure 2.**

Summary of formulae used for total and partial (segmented) electron transit time calculation in virtual anode wells with "rollover" B field.

**Figure 3.**

Summary of equations for total electron recirculation ratio, and under mirror reflection (MR) and wiffle-ball (WB) operating modes, and formulae used for critical system radii (gyro, adiabaticity, transition and magnetic pressure balance radii) in "rollover" wells.

**Figure 4. a,b**

Electron recirculation,  $G_j$ , vs.  $Z$  for various values of  $W$ . a) Non-diamagnetic case, no shift in  $\langle r_{ad} \rangle$  with increasing  $\langle r_b \rangle$ . b) Diamagnetic shift overestimated to show maximum effect.

**Figure 5. a-f**

Effect of well depth,  $\alpha_q$ , on  $G_j$  vs.  $Z$  plots for various values of  $W$ . The  $\langle r_b \rangle = 1$  line is indicated in each chart by the dashed line.

**Figure 6. a-d**

Effect of gyro "hole" radius,  $k_L$ , on  $G_j$  vs.  $Z$  plots for various values of  $W$ . a) The  $\langle r_b \rangle = 1$  line for  $k_L = 1, 2, 3$ . The magnitude of  $W$  at  $G_j = 1$  is indicated. b-d) Plot of  $G_j$  vs.  $Z$  for each value of  $k_L$  at  $\alpha_q = 1$ .

**Figure 7. a-d**

Effect of repeller efficiency,  $\alpha_r$ , on  $G_j$  vs.  $Z$  plots for various values of  $W$ .

**Figure 8. a-c**

3-D plots of 2-D projections for various repeller efficiencies, as in Figure 7, with  $k_L = 2$ .

## REFERENCES

- <sup>1</sup>Robert W. Bussard and Katherine E. King, "Electron Recirculation in Electrostatic Multicusp Systems: I - Confinement and Losses in Simple Power Law Wells," Energy/Matter Conversion Corp., Technical Report, EMC2-0491-03
- <sup>2</sup>I. Spalding, "Cusp Containment," in *Advances in Plasma Physics*, Vol. x, 1971, pp. 79-123
- <sup>3</sup>D.G. Blondin and T.J. Dolan, "Equilibrium plasma conditions in electrostatically plugged cusps and mirrors," *Jour. Appl. Phys.* Vol. 47, No. 7, July 1976, pp. 2903-2906
- <sup>4</sup>P.J. Catto and J.B. Taylor, "Electrostatic Enhancement of Mirror Confinement," *Nuclear Fusion*, Vol. 24, No. 7, (1984) pp. 229-233
- <sup>5</sup>O.A. Lavrent'ev, "Electrostatic and Electromagnetic High-Temperature Plasma Traps," Conference Proceedings, Electrostatic and Electromagnetic Confinement of Plasmas and the Phenomenology of Relativistic Electron Beams, Ann. N.Y. Acad. of Sci., Vol. 251, 1975, pp. 152-178
- <sup>6</sup>J. Berkowitz, et al, "Cusped Geometries," Proceedings of the Second International Conference on the Peaceful Uses of Atomic Energy, Geneva, 1958, United Nations, Geneva, Vol. 31, 1958, pp.171-176
- <sup>7</sup>R.W. Bussard, "Method and Apparatus For Controlling Charged Particles," U.S. Patent Number 4,826,626, May 2, 1989, assigned to Energy/Matter Conversion Corporation (EMC2)
- <sup>8</sup>R.W. Bussard, G.P. Jellison and G.E. McClellan, "Preliminary Research Studies of a New Method for Control of Charged Particle Interactions," Pacific-Sierra Research Corp. Report No. PSR-1899, 30 Nov. 1988, Final Report under Contract No. DNA001-87-C-0052, Defense Nuclear Agency, Sect. 1
- <sup>9</sup>R.W. Bussard, "Some Physics Considerations of Magnetic Inertial-Electrostatic Confinement: A New Concept for Spherical Converging-Flow Fusion," *Fusion Technology*, Vol. 19, No. 2, March 1991, pp. 273-293, Sect. III-C
- <sup>10</sup>Taylor, J.B. 1966, Culham Laboratory Rep. CLM R58
- <sup>11</sup>Grossman, W.B. 1966, *Physic Fluids*, 9, 2472
- <sup>12</sup>Kaye, A.S., "Plasma Losses Through an Adiabatic Cusp," *J. Plasma Physics*, Vol. 11, part 1, 1974, pp. 77-91
- <sup>13</sup>H. Grad, "Containment in Cusped Plasma Systems," in *Progress in Nuclear Energy, Series XI, Plasma Physics and Thermonuclear Research*, Vol. 2, ed. by C.L. Longmire, J.L. Tuck and W.B. Thompson, Pergamon Press, 1963, pp. 189-200
- <sup>14</sup>op. cit ref. 12
- <sup>15</sup>N.A. Krall, "The Polywell<sup>tm</sup>, A Spherically Convergent Ion Focus Concept," Krall Associates, internal Technical Report, KA-90-45, Feb. 1991, to be published in *Fusion Technology* (1991)
- <sup>16</sup>R.W. Bussard and K.E. King, "Computer Modelling of SCIF Experiment Performance," Energy/Matter Conversion Corp., Technical Report, EMC2-0691-02
- <sup>17</sup>R.W. Bussard and K.E. King, "Electron Transit Time in Central Virtual Anode Wells," Energy/Matter Conversion Corp., internal Technical Note, EMC2-0291-03, Feb. 1991
- <sup>18</sup>Op cit ref. 7, Appendix C, p. 189, Figure 2-1, "Magnetic field along square face axis; truncated cube"

<sup>19</sup>N.A. Krall, "The Polywell<sup>tm</sup>, A Spherically Convergent Ion Focus Concept," Krall Associates, internal Technical Report, KA-90-45, Feb. 1991, to be published in Fusion Technology (1991)

<sup>20</sup>S.K. Wong, "Structure of the Polywell<sup>tm</sup> Magnetic Fields," Energy/Matter Conversion Corporation, internal Technical Report, EMC2-0391-04, Mar. 1991

<sup>21</sup> R.W. Bussard, "Comparison of Models and Computer Simulations of Single Particle Electron Confinement in Multicusp Polywell<sup>tm</sup> Systems," Energy/Matter Conversion Corp., internal Technical Note, EMC2-0391-02, Mar. 1991, Sect. III

<sup>22</sup>K. Maffei, "Single Particle Electron Confinement Study," Directed Technologies Inc., DTI internal technical note, Aug. 2, 1990

<sup>23</sup>S.K. Wong, et al, "Statistical Study of Single Particle Confinement in a Cusped Magnetic Field," Energy/Matter Conversion Corp., internal Technical Note, EMC2-0491-02, Apr. 1991

<sup>24</sup>Robert W. Bussard, "Physics Analysis of Data From Computer Study of Electron Motion," Energy/Matter Conversion Corp., Technical Report, EMC2-0491-05, April/May 1991

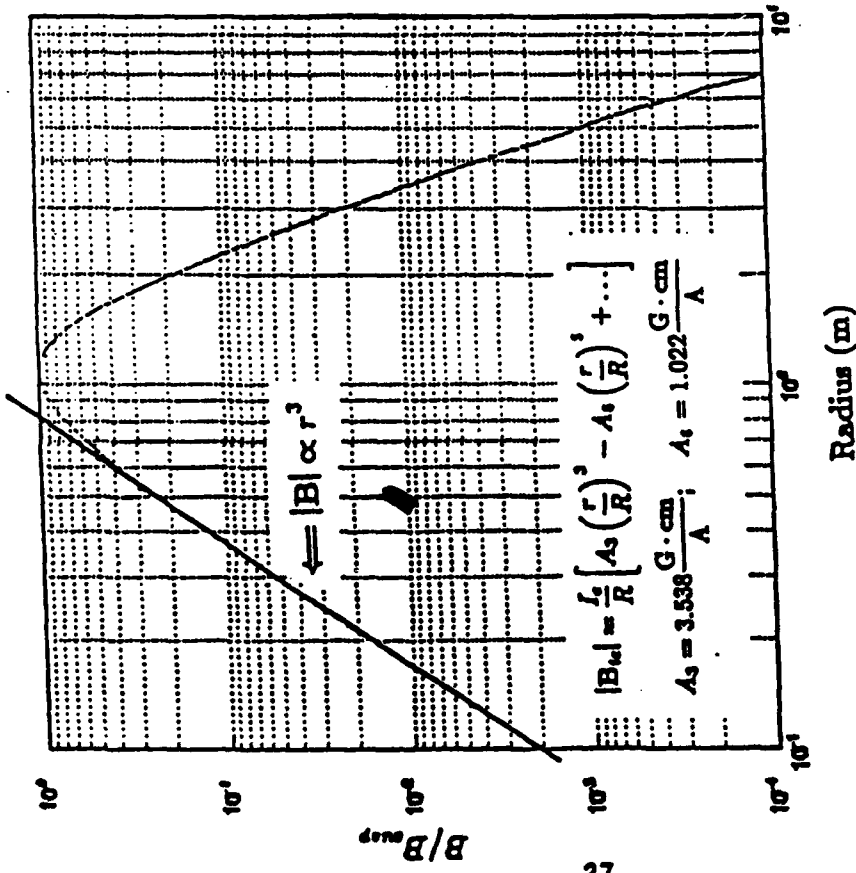
<sup>25</sup>N.A. Krall, "Density Profiles in the Polywell<sup>tm</sup>/SCIF Device," Krall Associates, internal Technical Report, KA-90-51, Dec. 1990

<sup>26</sup>Op cit ref. 8, Sect. VI-A

<sup>27</sup>Robert W. Bussard and Katherine E. King, "SCIF Performance from Code Calculations," Energy/Matter Conversion Corp., Technical Report EMC2-0691-02, June/July 1991

<sup>28</sup>Robert W. Bussard, "Effective Gyro Hole Loss Radius and Diamagnetic Limit in Polywell<sup>tm</sup> Systems," Energy/Matter Conversion Corp., Technical Report, EMC2-0591-02, May, 1991

<sup>29</sup>Robert W. Bussard, "SCIF Startup With Neutral Gas Background," Energy/Matter Conversion Corp., Technical Report, EMC2-0691-03, June/July 1991

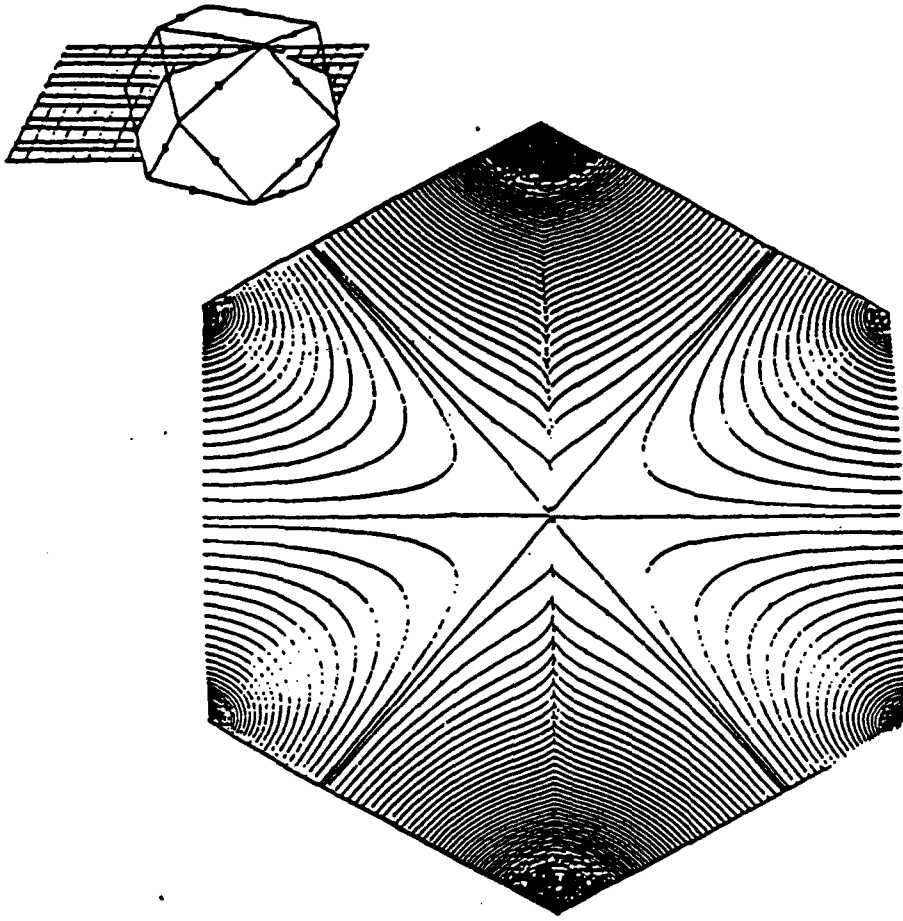


Magnitude of B

Lines of Force

Figure 1.

Variation of magnetic field in pure linear truncated cube systems, showing "rollover" at edge and field strength 2x higher in interior regions than used in simple power-law model normalized to square face edge strength.



Transit Time Calculations for  $G_{jo}$

$$t_{tot} = \frac{2R}{v_{in}} \left[ \frac{\langle r_0 \rangle + \left[ \frac{\langle r_w \rangle^2 - \langle r_0 \rangle^2}{2\langle r_0 \rangle} \right]}{\left[ \eta + \frac{\delta E_w}{2E_0} \right]^{1/2}} + \frac{2}{\left[ 1 + \frac{\delta E_w}{2E_0} \right]^{1/2}} \left[ \frac{1}{\langle r_w \rangle^{1/2}} - 1 \right] \right]$$

For  $\langle r_b \rangle < \langle r_w \rangle$ :

$$t_{MR} = \frac{2R}{v_{in}} \left[ \frac{\left[ \frac{\langle r_w \rangle^2 - \langle r_b \rangle^2}{2\langle r_0 \rangle} \right]}{\left[ \eta + \frac{\delta E_w}{2E_0} \right]^{1/2}} + \frac{2}{\left[ 1 + \frac{\delta E_w}{2E_0} \right]^{1/2}} \left[ \frac{1}{\langle r_w \rangle^{1/2}} - 1 \right] \right]$$

$$t_{WB} = \frac{2R}{v_{in}} \left[ \frac{\langle r_0 \rangle + \left[ \frac{\langle r_b \rangle^2 - \langle r_0 \rangle^2}{2\langle r_0 \rangle} \right]}{\left[ \eta + \frac{\delta E_w}{2E_0} \right]^{1/2}} \right]$$

For  $\langle r_b \rangle > \langle r_w \rangle$ :

$$t_{MR} = \frac{2R}{v_{in}} \left[ \frac{2}{\left[ 1 + \frac{\delta E_w}{2E_0} \right]^{1/2}} \left[ \frac{1}{\langle r_b \rangle^{1/2}} - 1 \right] \right]$$

$$t_{WB} = \frac{2R}{v_{in}} \left[ \frac{\langle r_0 \rangle + \left[ \frac{\langle r_w \rangle^2 - \langle r_0 \rangle^2}{2\langle r_0 \rangle} \right]}{\left[ \eta + \frac{\delta E_w}{2E_0} \right]^{1/2}} + \frac{2}{\left[ 1 + \frac{\delta E_w}{2E_0} \right]^{1/2}} \left[ \frac{1}{\langle r_w \rangle^{1/2}} - \frac{1}{\langle r_b \rangle^{1/2}} \right] \right]$$

$$\eta_0 = \frac{E_{ao}}{E_0} \quad \eta' = 1 - \alpha_q (1 - \eta_0) \quad \langle r_w \rangle \approx \langle r_0 \rangle + \left[ \frac{2}{m} \langle r_0 \rangle^2 \eta' \right]^{1/(m+2)}$$

$$\frac{\delta E_w}{2E_0} = \frac{1}{2} \left[ \langle r_w \rangle^m + \frac{\langle r_0 \rangle^2 \eta'}{\langle r_w \rangle^2} \right] + \frac{1}{2}(1 - \alpha_q) - \frac{1}{2}(1 - \alpha_q)$$

Figure 2.

Summary of formulae used for total and partial (segmented) electron transit time calculation in virtual anode wells with "rollover" B field.

Mirror/Wiffle Model for  $G_{jo}$

$$G_{jo} = G_{jMRO} \left[ \frac{4}{N} \frac{(1-\langle r_b \rangle)}{(1-\alpha_r)} t_{MR} + \langle r_b \rangle t_{WB} \right] \frac{1}{t_{tot}} \quad r_b < r_x$$

$$G_{jo} = G_{jMRO} \left[ \frac{4}{N} \frac{(1-\langle r_b \rangle)}{(1-\alpha_r)} t_{MR} + G_{jWB} \langle r_b \rangle t_{WB} \right] \frac{1}{t_{tot}} \quad r_b > r_x$$

where:

$$G_{jMRO} = \frac{1}{\langle r_{ad} \rangle^m} [1 - \alpha_q (1 - \langle r_{ad} \rangle^m)] \quad r_b < r_{ad}$$

$$G_{jMRO} = \frac{1}{\langle r_b \rangle^m} [1 - \alpha_q (1 - \langle r_b \rangle^m)] \quad r_b > r_{ad}$$

$$G_{jWB} = \frac{2r_e Z}{Nk_L^2 S^2} \quad Z = 8\pi n_c r_c^2 \quad \text{and} \quad W = \frac{E_0}{B_0^2 R^2}$$

$$\langle r_b \rangle^{(2m+2)} = (ZW) \frac{[1 - \alpha_q (1 - \langle r_b \rangle^m)]}{[f_0(\langle r_b \rangle)]^2} \quad \langle r_g \rangle^2 = \left[ \frac{2WS^2}{r_e \langle r \rangle^{2m}} \right] \frac{[1 - \alpha_q (1 - \langle r \rangle^m)]}{[f_0(\langle r \rangle)]^2}$$

$$\langle r_x \rangle^{(2m+2)} = \left[ \frac{NWk_L^2 S^2}{2r_e} \right] \frac{[1 - \alpha_q (1 - \langle r_x \rangle^m)]}{[f_0(\langle r_x \rangle)]^2} \quad S^2 = \overline{\sin^2 \varphi}$$

$$\langle r_{ad} \rangle = \langle r_{ad0} \rangle + k_a (\langle r_b \rangle - \langle r_x \rangle) \quad k_a = \frac{\langle r_k \rangle - \langle r_{ad0} \rangle}{\langle r_k \rangle - \langle r_x \rangle}$$

$$\langle r_{ad0} \rangle^{(2m+2)} = \left[ \frac{2m^2 WS^2}{\Gamma_a^2 r_e} \right] [1 - \alpha_q (1 - \langle r_{ad0} \rangle^m)] \left[ 1 + \frac{\langle r_{ad0} \rangle f'_0(\langle r_{ad0} \rangle)}{m f_0(\langle r_{ad0} \rangle)} \right]$$

$$f_0(\langle r \rangle) = \left[ \frac{2}{1 + \langle r \rangle^{(m+2)}} \right] \quad f'_0(\langle r \rangle) = - \frac{2(m+2)\langle r \rangle^{(m+1)}}{[1 + \langle r \rangle^{(m+2)}]^2}$$

Figure 3.

Summary of equations for total electron recirculation ratio, and under mirror reflection (MR) and wiffle-ball (WB) operating modes, and formulae used for critical system radii (gyro, adiabaticity, transition and magnetic pressure balance radii) in "rollover" wells.

Figure 4. a

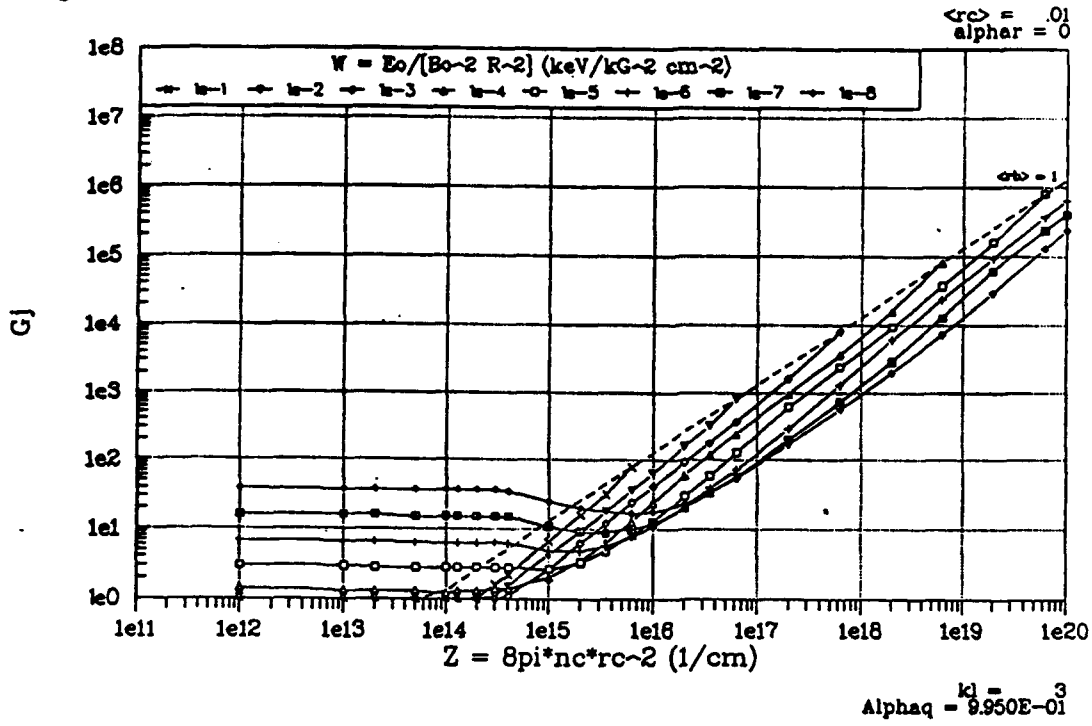


Figure 4. b

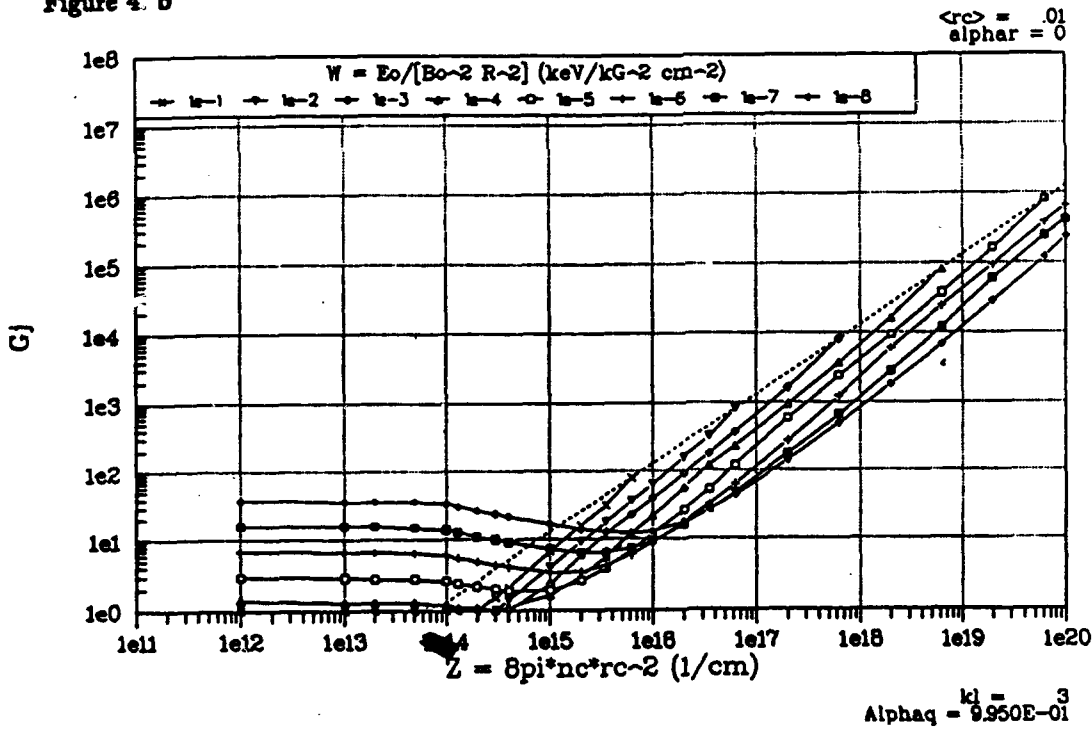
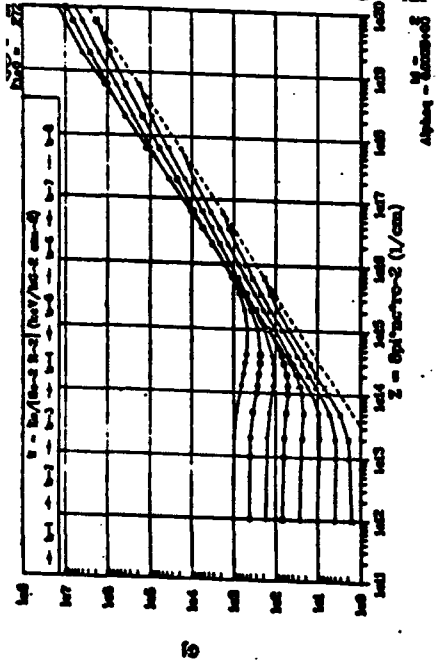


Figure 4. a,b

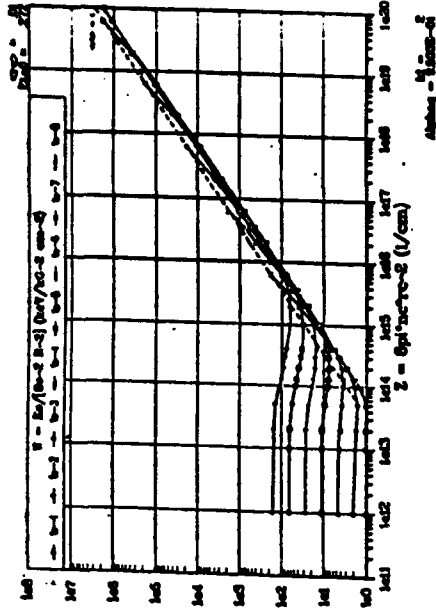
Electron recirculation,  $G_j$  vs.  $Z$  for various values of  $W$ . a) Non-diamagnetic case, no shift in  $\langle r_{ad} \rangle$  with increasing  $\langle r_b \rangle$ . b) Diamagnetic shift overestimated to show maximum effect.

Figure 5. a



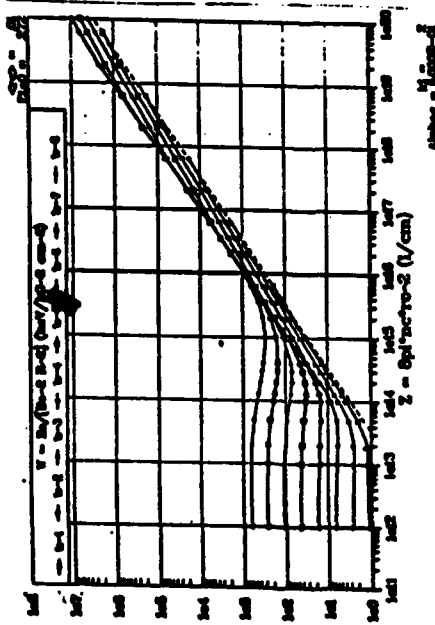
5

Figure 5. d



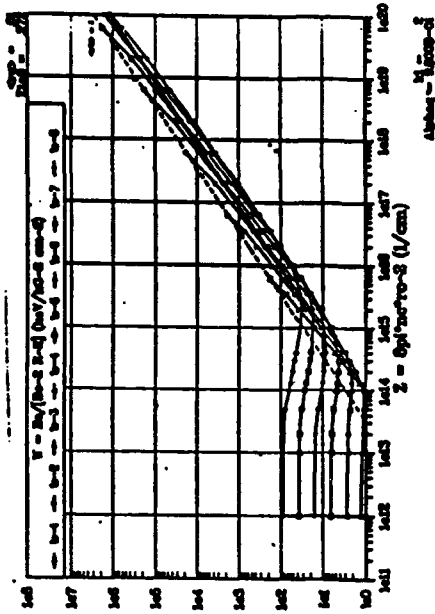
5

Figure 5. b



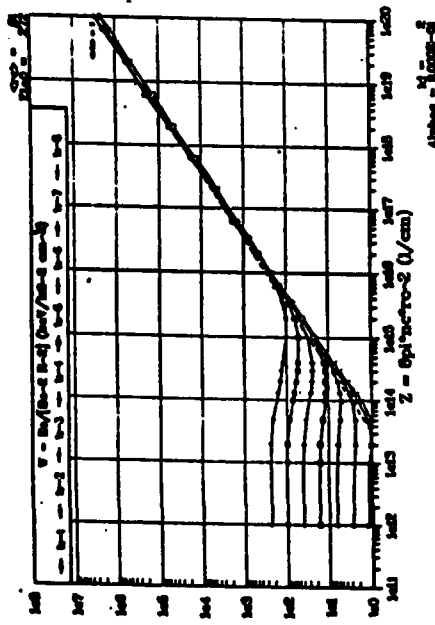
5

Figure 5. c



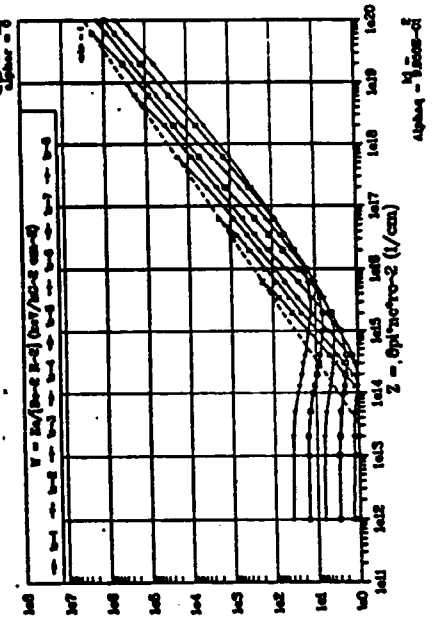
5

Figure 5. c



5

Figure 5. f



5

Figure 5. a-f

Effect of well depth,  $\alpha_j$ , on  $G_j$  vs.  $Z$  plots for various values of  $W$ . The  $\langle r_b \rangle = 1$  line is indicated in each chart by the dashed line.

Figure 6. a

$\langle r_b \rangle = 1$  for various values of  $k_L$   
 $W$ , as indicated, =  $E_0/[B_0^{-2} R^{-2}]$  (keV/kG<sup>-2</sup> cm<sup>-2</sup>)

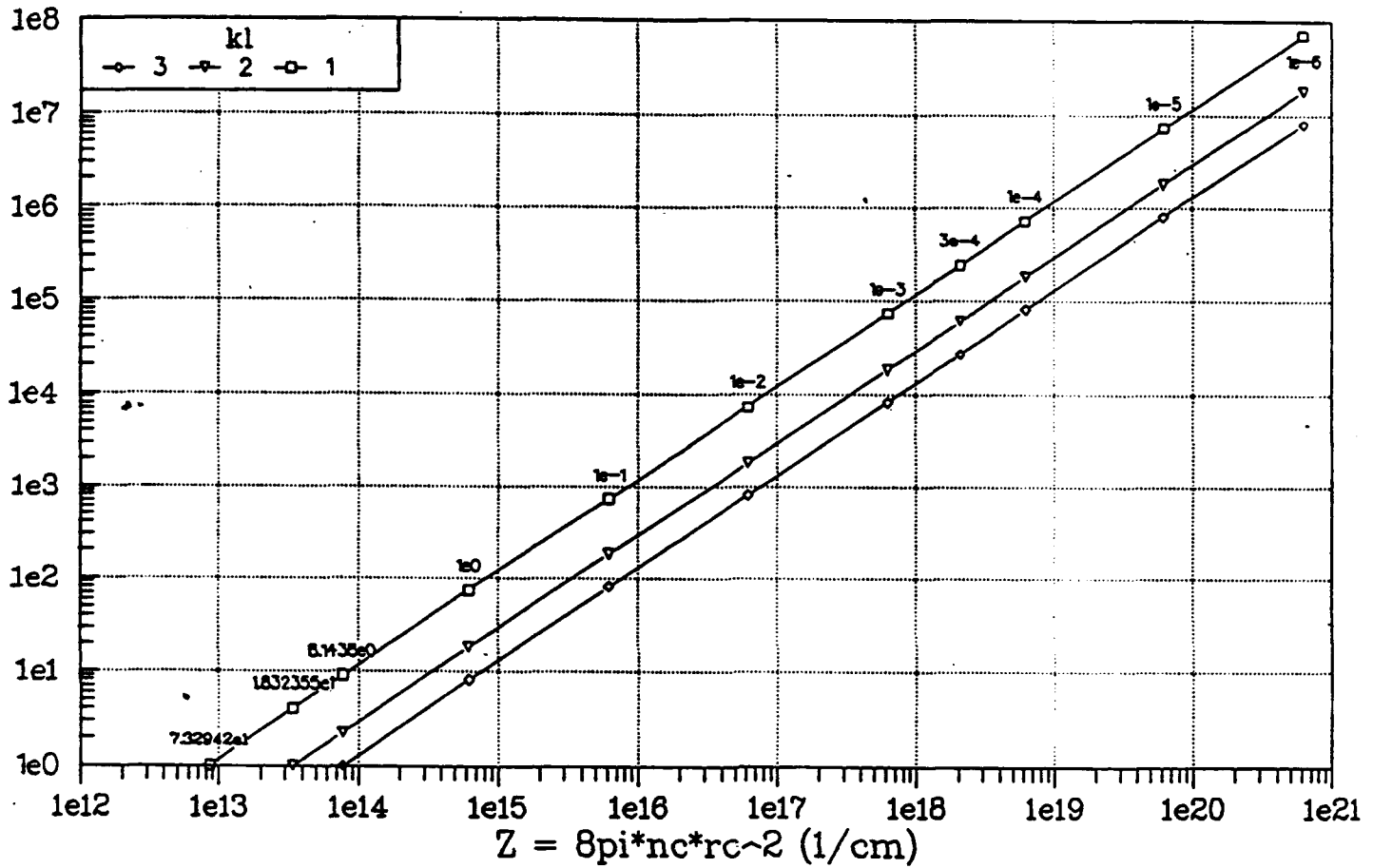


Figure 6. a-d

Effect of gyro "hole" radius,  $k_L$ , on  $G_j$  vs.  $Z$  plots for various values of  $W$ . a) The  $\langle r_b \rangle = 1$  line for  $k_L = 1, 2, 3$ . The magnitude of  $W$  at  $G_j = 1$  is indicated. b-d) Plot of  $G_j$  vs.  $Z$  for each value of  $k_L$  at  $\alpha_q = 1$ .

Figure 6. b

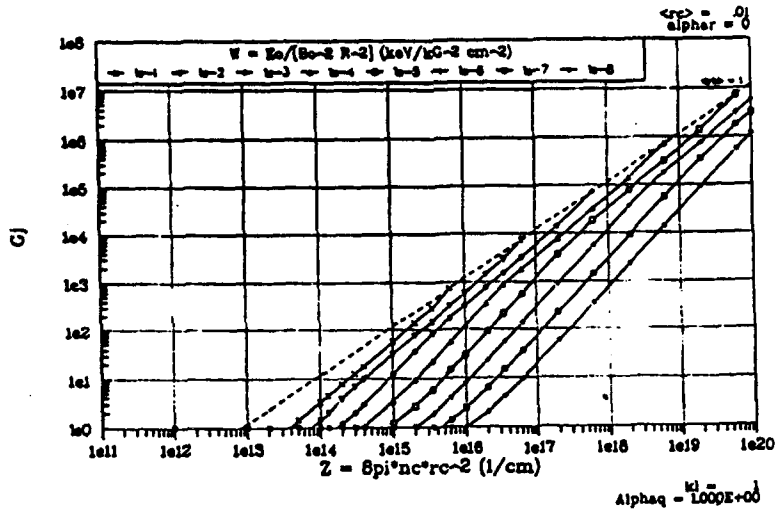


Figure 6. c

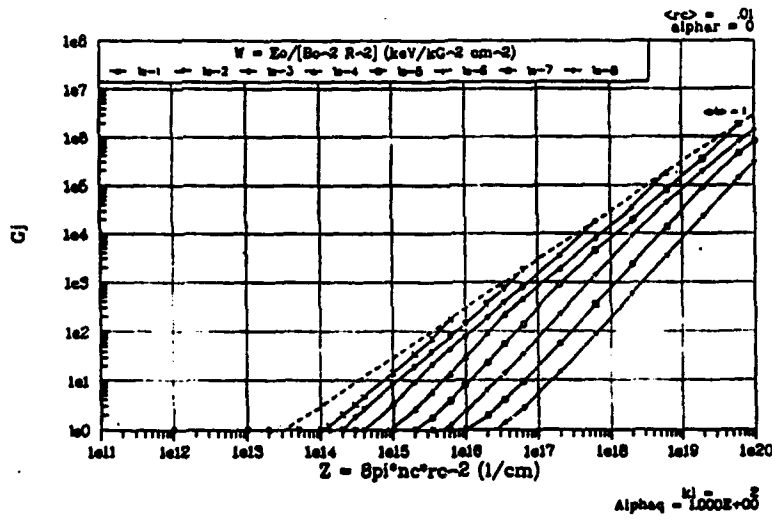
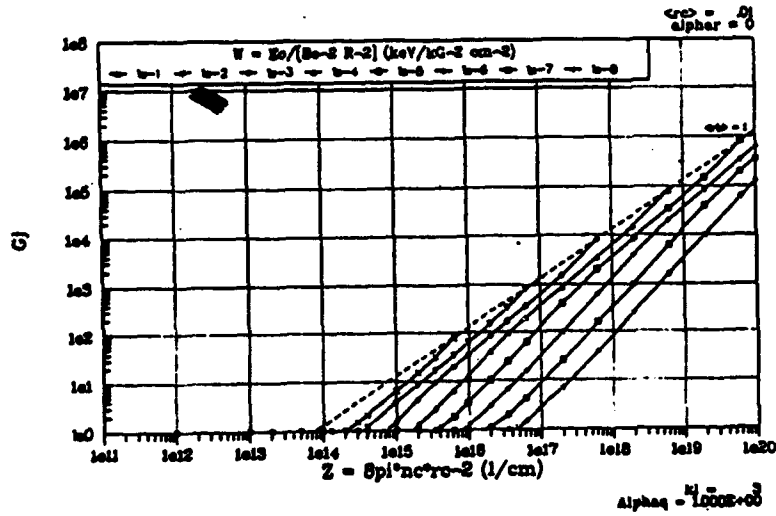


Figure 6. d



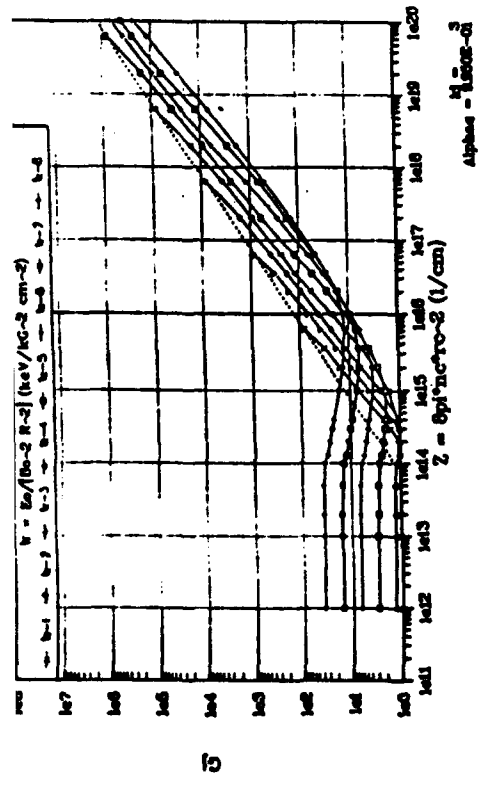


Figure 7. a

Figure 7. b

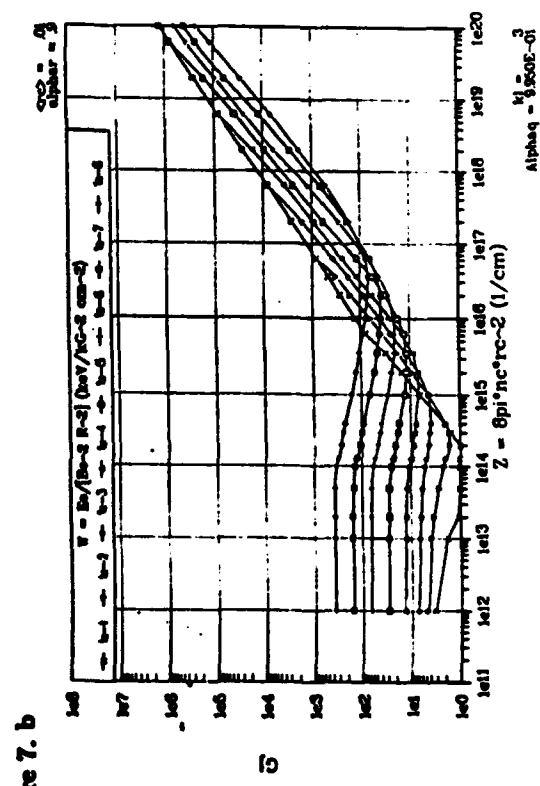


Figure 7. c

Figure 7. d

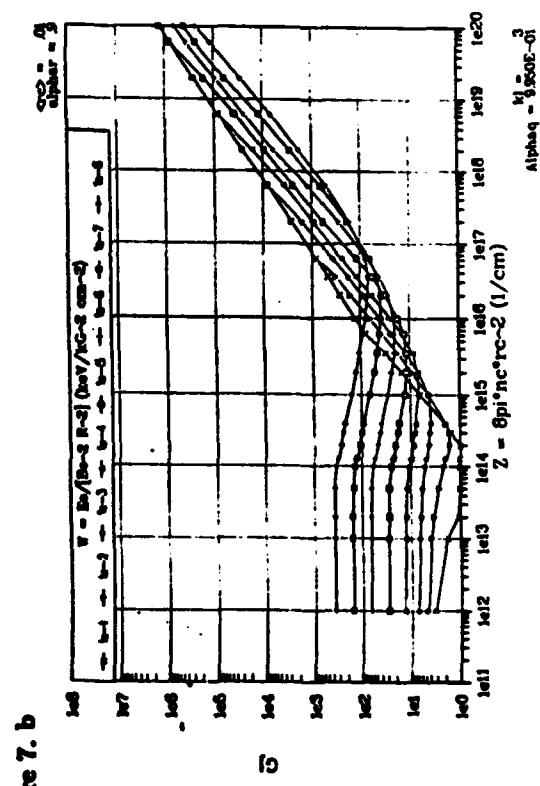
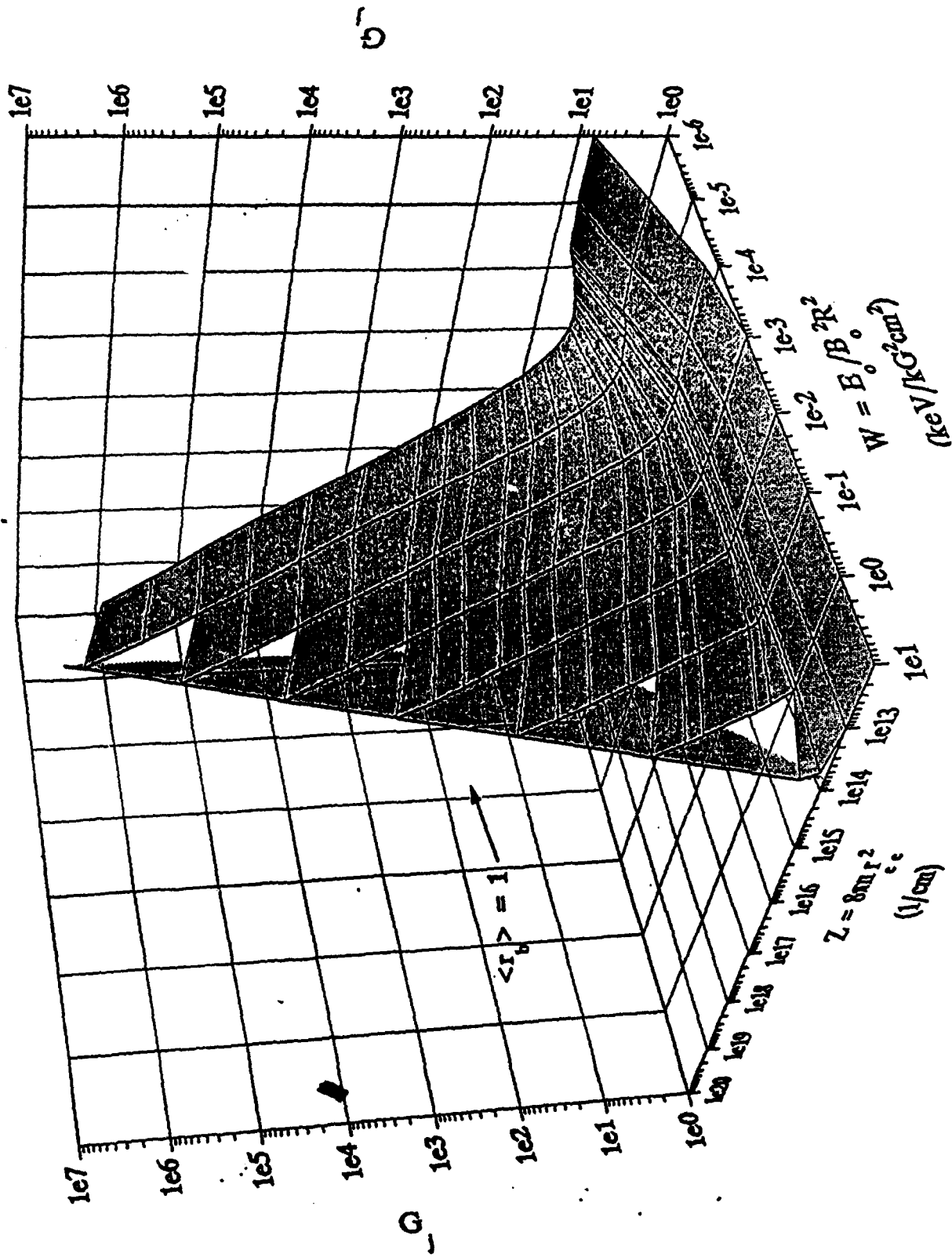


Figure 7. a-d  
Effect of repeller efficiency,  $\alpha_r$ , on  $G_j$  vs.  $Z$  plots for various values of  $W$ .

$$k_L = 2, \alpha_r = 0, \alpha_q = 0.995,$$

$$\eta = 0.272, m = 3, N_{VR} = N_{MR} = 8$$

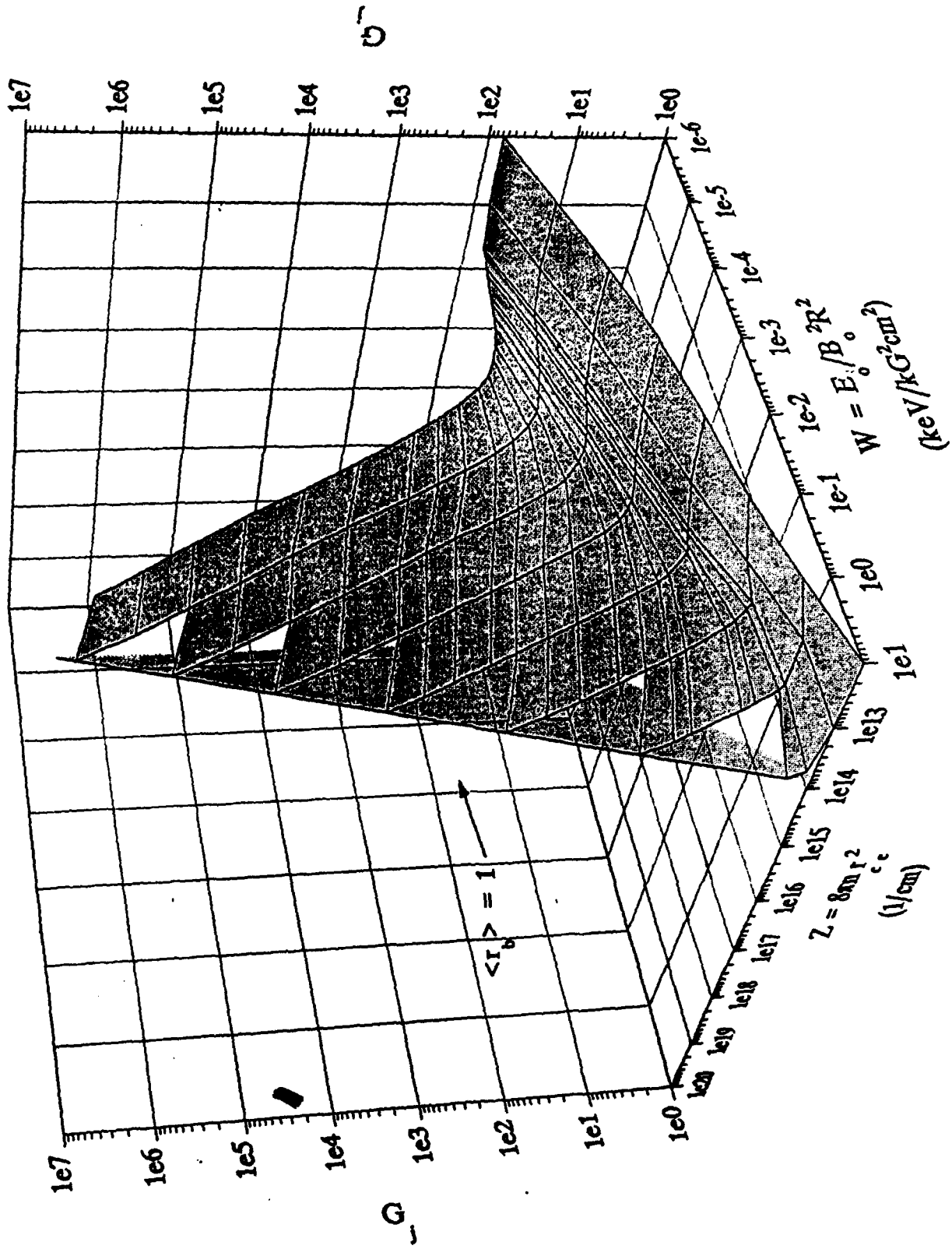
Figure 1. 3-D plot of 2-D projection for repeller efficiency  $\alpha_r = 0$ , with  $k_L = 2$ .



3-D plot of 2-D projection for repeller efficiency  $\alpha_r = 0.9$ , with  $k_L = 2$ .

$$k_L = 2, \alpha_r = 0.9, \alpha_q = 0.995,$$

$$\eta = 0.272, m = 3, N_{WA} = N_{MR} = 8$$



$k_L = 2, \alpha_r = 0.99, \alpha_q = 0.995,$   
 $\eta = 0.272, m = 3, N_{VR} = N_{MR} = 8$

Figure 8. c  
 3-D plot of 2-D projection for repeller efficiency  $\alpha_r = 0.99$ , with  $k_L = 2$ .

